Prediction of structures and gel transitions in systems of colloids with moderate-range attractions

2007 J. Phys.: Condens. Matter 19 036102

(http://iopscience.iop.org/0953-8984/19/3/036102)

INSTITUTE OF PHYSICS PUBLISHING JOURNAL OF PHYSICS: CONDENSED MATTER

J. Phys.: Condens. Matter **19** (2007) 036102 (16pp) doi:10.1088/0953-8984/19/3/036102

Prediction of structures and gel transitions in systems of colloids with moderate-range attractions

B Ahlström and J Bergenholtz

Department of Chemistry, Göteborg University, SE-412 96, Göteborg, Sweden

E-mail: jbergen@chem.gu.se

Received 15 September 2006, in final form 13 November 2006
Published 3 January 2007
Online at stacks.iop.org/JPhysCM/19/036102

Abstract

Predictions of glass transitions from the idealized mode-coupling theory (MCT) are tested for systems with intermediate-range particle attractions. Liquid structure input to MCT is provided by the Asakura–Oosawa (AO) theory for the depletion interaction, used as an idealized model for structures in colloid–polymer mixtures. The effective one-component formulation of the AO theory is verified to capture the complete pair structure found from the binary version of the theory also for polymer–colloid size ratios somewhat larger than those for which an exact mapping of the two descriptions holds. The Percus–Yevick theory is shown to provide an accurate structural input to MCT, at least in the single-phase fluid region. With this combination of theories, very reasonable predictions for locations of glassy states in the experimental phase diagram are obtained for polymer–colloid size ratios somewhat larger than have been considered before. Simple approximations are also suggested for extracting the remaining pair structure from calculations of the one-component AO theory.

1. Introduction

Colloidal particles interacting with moderately strong attractions can undergo both equilibrium and non-equilibrium transitions. While the former is well known, an example of the latter is physical gelation, associated with systems of colloidal particles acquiring solid-like properties despite remaining disordered structurally and in which particle 'bonds' are significantly reversible. This type of gelation in colloidal systems appears to be a common phenomenon. It has been observed experimentally in several different colloid systems. Examples of gel-forming systems include dispersions of sterically stabilized colloids, solutions of star polymers and block copolymer micelles, either in marginal solvents [1–5] or interacting via the depletion interaction in the presence of additives like non-adsorbing polymers [6–9].

Building on the success of applying the idealized mode-coupling theory of glassy dynamics [10–12] to hard-sphere colloids [13–17], it has more recently been tested for systems of attractive colloids. This has been met by a considerable degree of success. It not only captures a number of properties of these structurally arrested systems qualitatively, such as large non-ergodicity parameters and a viscoelastic solid response, but it also predicts complex structural arrest scenarios [18], which has led to a distinction between repulsive, hard-sphere-like glasses and attractive glasses [19–21]. MCT has also been tested, albeit to a lesser extent, in quantitatively reproducing locations of attractive glass/gel regions of experimentally determined phase diagrams, where agreement has seemingly been fair [19, 22, 23]. Recent studies [24–26], however, have shown that MCT predictions for systems associated with very small ranges of attraction err in that structural arrest is predicted in the (metastable) single-phase fluid region at low colloid concentrations, rather than phase separation followed by gelation. It remains unknown whether MCT can be used to model these low-density gel transitions, but proposals for applying MCT to situations when phase separation kinetics enter have been advanced [27, 28].

The most extensive testing of the predictive ability of MCT for attractive colloids has been for model systems of colloid–polymer mixtures, for which the colloid–colloid interaction is of the depletion type [8]. Here, the polymer–colloid size ratio ξ determines the range of the attraction and is particularly pivotal in that it controls the topology of the equilibrium phase diagram [7, 29–32]. With a few exceptions [33], tests of MCT or related theories for predicting low-density gel transitions or higher-density attractive glass transitions have been made for small values of the size ratio, $\xi < 0.1$, i.e. for short-range attractions. For sufficiently small ξ, the theory can be simplified by an asymptotic analysis to yield analytical predictions [22, 23, 34, 35]. Unfortunately, for larger ranges of attraction similar simplifications are not possible, and full numerical solutions are required.

In this work we aim to make comparisons with phase diagrams determined for moderately ranged attractions, corresponding to larger values of ξ, but still sufficiently small that gel states have been recorded experimentally. Essentially we take the extension of the MCT glass transition, akin to the attractive glass branch at smaller ξ [18, 19, 23], as a model for locating the gel states observed experimentally. As these occur in regions where one expects a metastable binodal, we aim to see to what extent the MCT predictions for the glass transition can be used to locate them in the phase diagram. We pursue a fully predictive modelling, relying on integral equation theory predictions of the static structure to serve as input in MCT. The accuracy of the static input is tested through comparisons with Monte Carlo simulations, where we pay special attention to making sure that the one-component Asakura–Oosawa (AO) theory gives a faithful representation of the complete microstructure. For the simple model of ideal polymer spheres, pair-wise additivity of the AO potential remains accurate despite not being fulfilled rigorously, and Percus–Yevick (PY) theory is shown to capture liquid structures nearly quantitatively in the one-phase fluid region.

In what follows, we begin by briefly reviewing both the two-component and the effective one-component descriptions of the AO interaction, restricting the analysis to ideal polymers. We outline the method of computer simulation, followed by comparisons of the static structure from simulation and from PY theory. We pay particular attention to evaluation of the structures as obtained from PY theory because we apply the one-component description for values of ξ where it is not an exact mapping of the binary AO system. In this context, we also make sure that the polymer component is modelled in a reasonably accurate manner. Finally, the colloid–colloid static structure factor is substituted in MCT, the predictions of which we compare with experimental phase diagram data.

2. Depletion interaction for ideal polymers

The depletion interaction arises in colloidal dispersions when adding for instance non-adsorbing polymers. It manifests itself as an effective interaction within a one-component description of a system of colloids and polymers. For ideal polymer spheres mixed with hard-sphere colloids, when the size ratio $\xi = \sigma_p/\sigma_c \leqslant 2/\sqrt{3} - 1 \approx 0.1547$ [29], the system is governed by pair-wise additivity of the AO potential [36–38],

$$\phi_{AO}(r) = \begin{cases} \infty & r < \sigma_c \\ -\Pi_p \times \dfrac{\pi}{6}\sigma_c^3(1+\xi)^3 & \\ \quad \times \left(1 - \dfrac{3}{2}\left(\dfrac{r/\sigma_c}{1+\xi}\right) + \dfrac{1}{2}\left(\dfrac{r/\sigma_c}{1+\xi}\right)^3\right) & \sigma_c < r < \sigma_c(1+\xi) \\ 0 & \sigma_c(1+\xi) < r \end{cases} \tag{1}$$

where σ_p and σ_c are diameters of polymers and colloids, respectively, and r is the separation distance. The size ratio determines the range of the attraction and the osmotic pressure of the polymer solution Π_p determines the magnitude of the attraction. In this description, the polymers are assumed to be ideal and the osmotic pressure is given by van't Hoff's law, $\Pi_p = n_p^r k_B T$. It is, however, important that the number density be based on the volume available to the polymers as indicated by the superscript [7, 32].

Alternatively, the same system can be described as a non-additive binary hard-sphere mixture [38, 39]. The colloids are modelled as hard spheres whereas the polymers are treated as ideal, penetrable to one another, but with a hard-sphere interaction with respect to the colloids, i.e.

$$\phi_{cc}(r) = \begin{cases} \infty & r < \sigma_c \\ 0 & r > \sigma_c \end{cases} \tag{2}$$

$$\phi_{cp}(r) = \begin{cases} \infty & r < \sigma_{cp} \\ 0 & r > \sigma_{cp} \end{cases} \tag{3}$$

$$\phi_{pp}(r) = 0 \tag{4}$$

where $\sigma_{cp} = (\sigma_c + \sigma_p)/2$. For small size ratios, $\xi \leqslant 0.1547$, all three- and higher-body contributions to the effective potential vanish [29] and these two descriptions become equivalent provided the mapping between them is done in a self-consistent way [40]. The key parameter in this context is the free-volume fraction $\alpha = \eta_p/\eta_p^r$ of such an idealized colloid–polymer mixture, relating the polymer volume fractions η_p and η_p^r to one another. The free-volume fraction depends not only on the volume fractions but also implicitly on the colloid structure as [40]

$$\alpha = \frac{\eta_p}{\eta_p^r} = 1 - \eta_c(1+\xi)^3 - \frac{12\eta_c^2\xi^3}{\eta_p^r}\int_1^{1+\xi} \mathrm{d}r\, r^2 g_{cc}(r;\eta_c,\eta_p^r)\beta\phi_{AO}(r) \tag{5}$$

where r is here non-dimensional on σ_c, and $g_{cc}(r;\eta_c,\eta_p^r)$, the colloid–colloid radial distribution function, is obtained from a system of colloids interacting via the AO potential in equation (1).

3. Methods

All simulations were performed with the standard (canonical) NVT-Monte Carlo (MC) technique in a simulation box of unit size using periodic boundary conditions [41]. One MC cycle corresponds to one attempt to move all particles sequentially [42]. The maximum

displacement step length was adjusted to reach an acceptance ratio of about 50% during the equilibration phase, but it was kept fixed during production runs [43]. Simulations of the one-component system interacting with the AO potential were performed with 4000 particles, starting from an fcc lattice. They were equilibrated for at least 5×10^4 MC cycles and the production phases were run for at least 10^4 MC cycles (5×10^4 cycles for determinations of structure factors), accumulating averages every 50 cycles.

The binary mixture simulations were started from a total of 10 000 particles randomly placed in the simulation box, except for the composition ($\eta_c = 0.35$, $\eta_p = 0.05$) for which 5000 particles were used. Since the total number of particles is the sum of colloids and polymers, the number of colloids ranged from 78 to 519 for the compositions explored in this work. These systems are difficult to equilibrate, owing to the inefficient sampling of configuration space. Root mean square displacements of at least one box length during equilibration and one half box length during production runs were imposed, in addition to monitoring the radial distribution function, for approach to equilibrium.

The one-component PY theory was solved numerically for the AO potential using the algorithm in [44]. The resulting colloid–colloid structure factors were subsequently used in MCT to generate predictions for glass transitions. The long-time limit of the MCT equations was solved in discretized form numerically by iteration on a wavevector grid with a resolution given by $k = N\Delta k$, where $N = 900$ and $\Delta k \approx 0.2\sigma_c^{-1}$. The limiting compositions that yield non-zero solutions for the dynamic structure factor were identified by bracketing and were used to locate glass transitions in the phase diagram.

4. Results and discussion

4.1. Liquid structure

We have compiled simulation data for the AO model with $\xi = 0.25$ for a number of polymer–colloid compositions. Values close to this size ratio have been studied in several experiments [7, 28, 45–47] and by computer simulation [48–51]. Perturbation [29, 31, 52], free-volume [7, 32, 53, 54], integral equation [55], and density functional theories [56, 57] have also been applied to model the phase behaviour of colloid–polymer mixtures. In particular, Ilett and co-workers [7] employed polymer–solvent solutions at slightly-better-than-theta conditions in their experiments, making an attempted comparison with results derived from AO theory reasonable, at least for not too large values of ξ. Ilett *et al* in addition identify gel structures where the dynamics becomes non-ergodic. We propose to use MCT based on AO model static structures to predict their location in the experimental phase diagram. To this end, we first verify that the one-component description remains an accurate representation of the binary AO model. We do this by examining the complete microstructure at the pair level. Moreover, in pursuing a predictive model, we test the integral equation theory against simulation results for a relatively broad range of parameters.

As shown in the inset to figure 1, we have explored a large portion of the single-phase part of the phase diagram for the AO system used in this work. The simulated compositions, indicated by filled circles, are given in terms of the volume fractions of polymers and colloids, η_p and η_c. At sufficiently large concentrations of polymer, colloid–colloid radial distribution functions develop a shoulder in the structure just before the second peak. We interpret this signature as a precursor to crystallization [58], and we confine most of our comparisons to compositions where this is not observed (see the inset to figure 1). But it is worth noting that the order parameters for crystallization, Q_4 and Q_6 [59], were not particularly large (in all cases <0.07) for compositions where the shoulder was clearly observed [60].

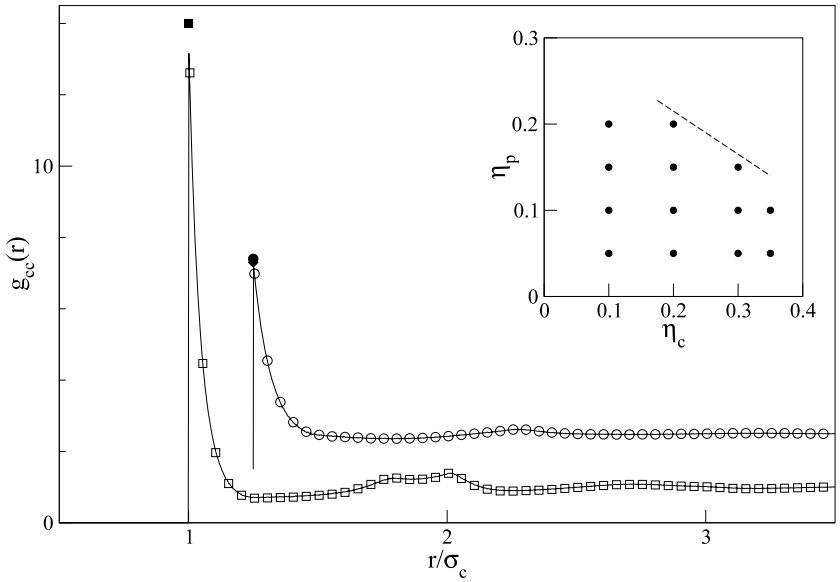

Figure 1. The colloid–colloid radial distribution function $g_{cc}(r)$ as a function of the separation normalized by the colloid diameter. The lines correspond to MC simulation of the binary mixture and the symbols to MC simulations of the effective one-component system interacting via the AO potential for $\xi = 0.25$, $\eta_c = 0.30$ with $\eta_p = 0.10$ (line, circles, offset vertically by $+3/2$ for clarity) and $\eta_p = 0.20$ (line, squares), yielding $\eta_p^r = 0.22$ and 0.42, respectively. Filled symbols mark extrapolated values for the radial distribution functions at contact. The inset shows compositions explored in this work where the line indicates the approximate location beyond which signs of phase separation were noted.

In what follows, except when noted, all work is done for a size ratio $\xi = 0.25$. For this size ratio the non-additive binary hard-sphere mixture cannot be mapped rigorously onto the effective one-component system consisting of colloids interacting in a pair-wise additive manner via the AO potential. However, it is expected that the size ratio is small enough for pair-wise additivity to remain accurate [48, 49]. We verify this by comparing liquid structures obtained from MC simulation of the binary and effective one-component models. As an example, in figure 1, comparisons are shown for $\eta_c = 0.30$ with $\eta_p = 0.10$ and 0.20 (yielding $\eta_p^r = 0.22$ and 0.42, respectively), where the connection between the one- and two-component descriptions is made via equation (5). As can be seen, the two determinations from the simulations using the different descriptions agree closely, both concerning the overall shape and also in the contact value of the radial distribution function. At the higher polymer volume fraction in figure 1 the radial distribution function exhibits a shoulder in the second peak structure as mentioned above, which is well described by the one-component description.

The remaining radial (pair) distribution functions can be extracted from the one-component AO model by periodically inserting either one or two polymer spheres in the course of an MC simulation. This procedure is exact for small size ratios and errors stemming from non-pair-wise additivity of the AO potential are introduced when performed for larger size ratios, unless many-body colloid correlations are accounted for [61]. Here we use it to determine whether the mapping remains accurate for the complete pair-level structure for this size ratio. In essence, this probes higher-order correlation function, albeit in an indirect fashion (see the appendix). In figure 2 we compare $g_{cp}(r)$ and $g_{pp}(r)$ as obtained from the two different routes for the composition $\eta_c = 0.30$ and $\eta_p = 0.15$, resulting in $\eta_p^r = 0.328$. As seen, these

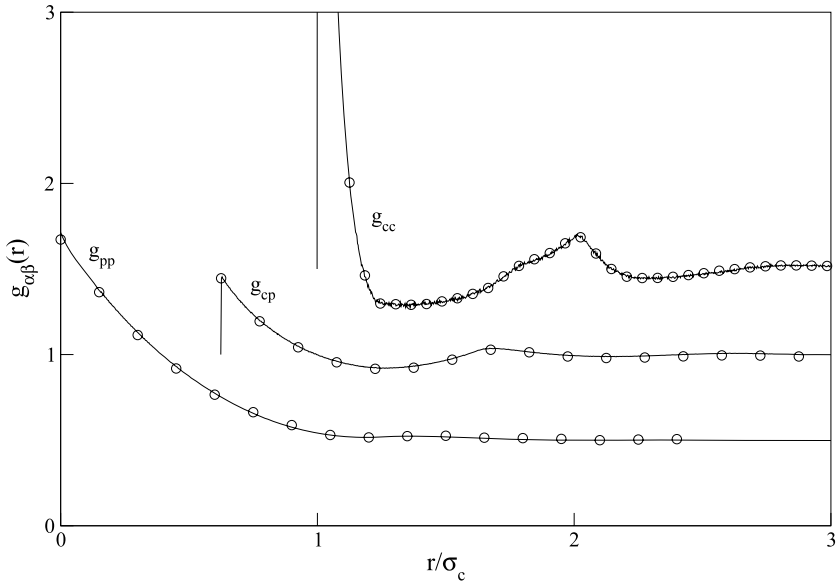

Figure 2. Radial distribution functions, g_{cc}, g_{cp}, and g_{pp}, as functions of separation normalized by the colloid diameter for $\xi = 0.25$, $\eta_c = 0.30$, $\eta_p = 0.15$, and $\eta_p^r = 0.328$. The lines correspond to data from MC simulation of the binary mixture and symbols to MC simulation of the one-component AO model. For clarity, g_{cc} and g_{pp} have been offset vertically by $\pm 1/2$.

radial distribution functions are also quantitatively reproduced by the effective one-component description, a result which holds for all compositions studied. It follows that for $\xi = 0.25$ pair-wise additivity of the AO potential is an excellent approximation, as expected also from the work of Meijer and Frenkel [48, 49].

The Percus–Yevick (PY) theory is generally the integral equation of choice for short-range interactions [62]. It has been applied in the past to study liquid structure both in the effective one-component [50] and the binary [63, 64] AO systems. In figure 3 we examine the PY prediction for the colloid–colloid radial distribution functions by comparing against results from simulation. In general, PY theory compares favorably for low to moderate polymer concentrations. As shown in the inset to figure 3, it does not reproduce the shoulder in the second peak structure that appears, presumably close to freezing, at higher polymer concentrations, but otherwise it captures the second peak structure well. In addition, and in contrast to the PY hard-sphere prediction, the theory tends to overestimate somewhat the contact values of the radial distribution function when the polymer concentrations is high. Overall, however, PY theory provides near-quantitative predictions for the colloidal microstructure in the single-phase fluid regime. It is then to be expected that it compares well in terms of the colloid–colloid structure factor, $S_{cc}(k)$, as is also seen to be the case in figure 4. Deviations between PY theory and simulation results for $S_{cc}(k)$ appear, however, when polymer concentrations become high, as shown in the inset to figure 4. As seen by the low-k upturn and the split in the second peak of the corresponding $g_{cc}(r)$ in figure 1, this composition should be close to a phase boundary. Indeed, as Lo Verso *et al* have found by a hierarchical reference theory [65], this composition is very close to the metastable binodal. We note also that in the region of the phase diagram where one expects a fluid–solid transition [65] the height of the primary structure factor peak reaches values nowhere near those expected from the Hansen–Verlet freezing criterion [62], as also previously noted for this system [50, 63].

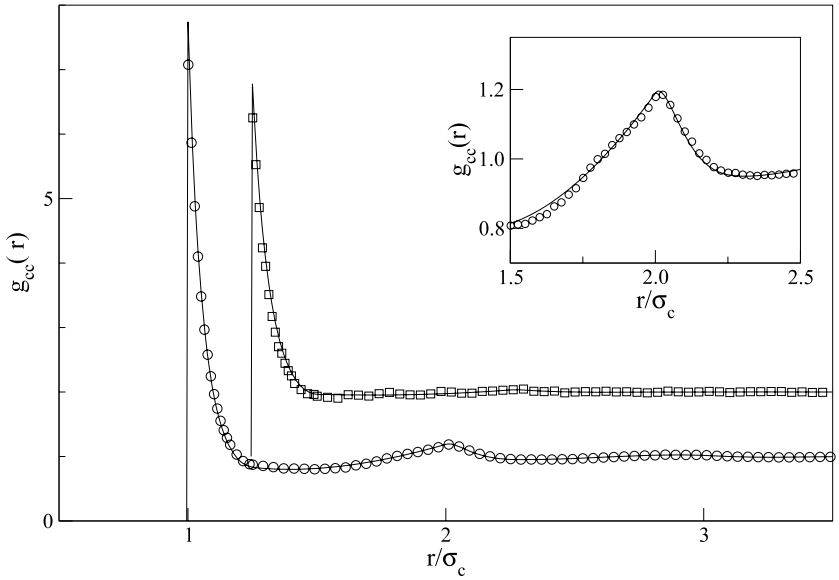

Figure 3. Comparison of colloid–colloid radial distribution function $g_{cc}(r)$ as a function of separation normalized by the colloid diameter from MC simulation of the two-component AO system (symbols) and PY theory for the one-component AO system (lines). Two compositions at $\xi = 0.25$ are shown: $\eta_c = 0.35$, $\eta_p = 0.10$, $\eta_p^r = 0.27$ (line, circles) and $\eta_c = 0.10$, $\eta_p = 0.20$, $\eta_p^r = 0.248$ (line, squares). For clarity, g_{cc} for the latter has been offset vertically by $+1$. The inset is an enhancement about the second peak for $\eta_c = 0.35$, $\eta_p = 0.10$, $\eta_p^r = 0.27$.

In the next section the structure factor is used as input in MCT for predictions of glass transitions.

While PY theory captures the liquid structure well for the one-component AO system, the two-component version does so only when the polymer concentration is kept low. It is readily seen that in the limit $\eta_c \to 0$, the two-component PY theory yields $g_{cc}(r) \approx 1 - \beta\phi_{AO}(r)$ in the range $\sigma_c < r < \sigma_c(1 + \xi)$ rather than $g_{cc}(r) \approx e^{-\beta\phi_{AO}(r)}$. It follows that accurate predictions are obtained only for low polymer concentrations, as observed by Dijkstra and co-workers [64]. To predict the remaining radial distribution functions, we propose to exploit the accuracy of the one-component PY theory in formulating simple approximations for $g_{cp}(r)$ and $g_{pp}(r)$. As discussed in the appendix, one such approximation is realized by calculating the radial distribution functions subject to the two-component PY closure with the added constraint that $g_{cc}(r)$ be determined by the one-component PY theory applied to the one-component AO model. In this prescription we rely on equation (5) to provide the connection between η_p, which appears in the two-component Ornstein–Zernike equations, and η_p^r, which is required for solving the one-component PY equation.

In figure 5 we compare results from this revised PY theory for the partial radial distribution functions with results from simulation. The theory is in good agreement with the simulation result for $g_{cp}(r)$ but underpredicts somewhat the result for $g_{pp}(r)$, where it fails to produce the expected result, $g_{pp}(0) = 1/\alpha$ [52]. A second, even more simple, approximation can be formulated, again by exploiting that accurate results are obtained for $g_{cc}(r)$ in the effective one-component system using the PY closure. As shown in the appendix, the remaining radial distribution functions can be expressed in terms of integrals over $g_{cc}(r)$, $g_{cp}(r)$, and higher-order correlation functions. For small size ratios only a few terms are non-zero, and,

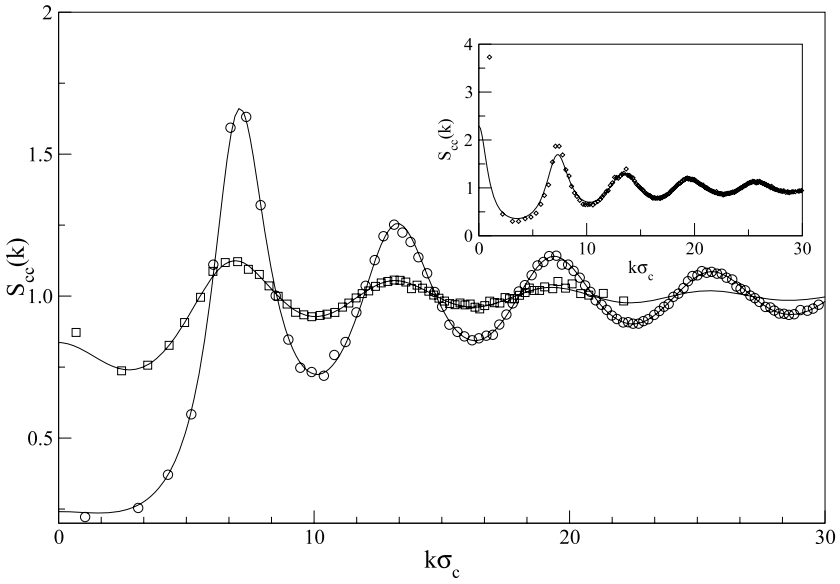

Figure 4. The colloid–colloid static structure factor S_{cc} as a function of the normalized wavevector $k\sigma_c$ for two different compositions, both with $\xi = 0.25$, as obtained from MC simulations of the effective one-component system interacting via the AO potential (symbols) and from the one-component PY theory (lines): $\eta_c = 0.35, \eta_p^r = 0.27$ (line, circles) and $\eta_c = 0.10, \eta_p^r = 0.248$ (line, squares). The inset shows the MC simulated $S_{cc}(k)$ (diamonds) for $\eta_c = 0.30$ and $\eta_p^r = 0.42$ together with the PY result (line). The corresponding simulation result for $g_{cc}(r)$ is given in figure 1.

moreover, one may expect that the leading-order terms dominate. Thus we approximate the radial distribution functions $g_{cp}(r)$ and $g_{pp}(r)$ by keeping just the first few terms involving only pair distribution functions, which can be determined easily by numerical integration once $g_{cc}(r)$ has been obtained from solution of the one-component PY theory. Figure 5 shows the predictions from this low-order approximation. As seen, they slightly overpredict the simulation results for the first correlation peak and are slightly low just prior to the second peak in $g_{cp}(r)$. For smaller size ratios, $\xi < 0.25$, the two approximations fall closer to one another. Similarly to figure 5, however, the revised integral equation underpredicts the simulation results for the small-r structure of $g_{pp}(r)$, whereas the low-order approximation overpredicts it. The predictions improve on the whole, however, with decreasing size ratio, but the integral equation theory appears to give better structural predictions.

4.2. Mode-coupling theory predictions

With the PY theory as input, we proceed to investigate the output of MCT. MCT gives a dynamic description of the glass transition. The theory emerges as a set of nonlinear equations for the dynamic structure factor $S(k, t)$ on closing the governing equations of motion. Self-consistent solutions of the equations require the static structure factor as input and yield the time and wavevector dependence of $S(k, t)$. Fluid states are characterized by a vanishing long-time limit: $S(k, t \to \infty) = 0$. For systems of strongly interacting particles, however, the equations exhibit bifurcations for $S(k, t \to \infty)$, such that $S(k, t \to \infty)$ acquires a non-zero value. Thus, glassy states arise in this idealized version of the theory as systems with an indefinite density correlation, leading to solid-like properties, yet systems remain disordered structurally.

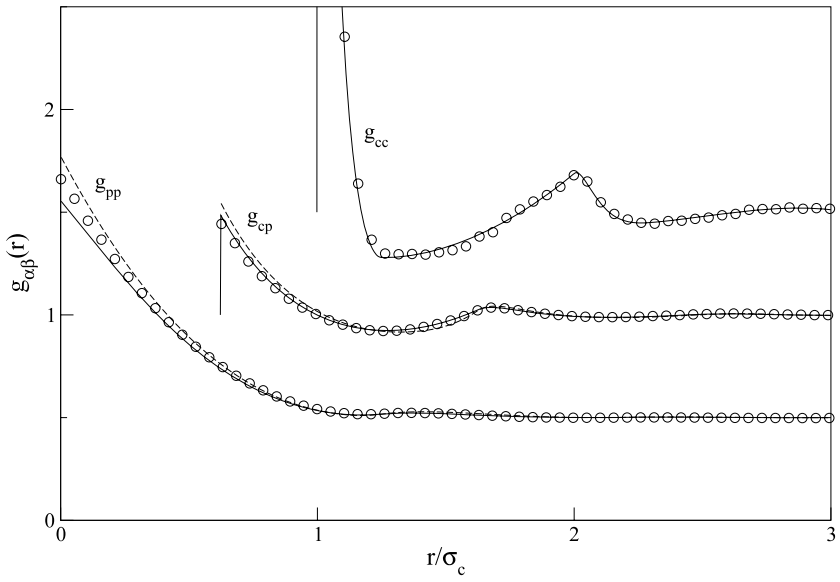

Figure 5. Radial distribution functions, g_{cc}, g_{cp}, and g_{pp}, as functions of separation normalized by the colloid diameter for $\xi = 0.25$, $\eta_c = 0.30$, $\eta_p = 0.15$, and $\eta_p^r = 0.328$. Circles are results from MC simulation of the binary mixture, the solid lines correspond to results from the revised PY theory, and the dashed lines are a low-order approximation. Both approximations are based on g_{cc} as obtained from the one-component PY theory (see the appendix). For clarity, g_{cc} and g_{pp} have been offset vertically by $\pm 1/2$.

In this study we use the colloid–colloid static structure factor $S_{cc}(k)$ from the one-component PY theory as input in MCT, which makes for a fully predictive theory for the AO interaction. Glass transitions are determined here from MCT as functions of colloid and polymer volume fractions for somewhat larger colloidal attraction ranges than have been considered before (see, however, related approaches by Chen and Schweizer [33]). In this case the transitions are simultaneously influenced by the cage effect and the moderate-range attraction and it is the task of MCT to gauge these effects in locating glass transitions. In addition, for these longer-ranged attractions MCT predicts transitions that traverse the phase diagram until they meet the spinodal on the liquid side. This prediction appears to be generic for colloidal systems, though MCT predicts otherwise for shorter-ranged attractions [22, 23, 34], as computer simulations find that no matter how short the range of attraction is made, structural arrest transitions meet the binodal on the liquid side [25]. Thus, for the situation at hand, MCT predictions agree at least qualitatively with this recent finding.

Results from combining PY and MCT theories are shown in figure 6, for size ratios of 0.20, 0.25, and 0.30, in terms of η_p^r and η_c. The inset shows the same results in the (η_p, η_c) representation. Spinodals were determined from PY theory using the compressibility route and the procedure suggested by Gallerani *et al* [66]. As seen, phase separation requires larger values of η_p^r or η_p the larger the size ratio is. This occurs because the well depth of the AO potential is governed mainly by the polymer number density rather than η_p^r, and it is qualitatively consistent with observations from experiments on sterically stabilized colloids mixed with non-adsorbing polymers close to theta conditions [7, 47]. Shah *et al* [47] have also noted a more subtle effect. The fluid–fluid binodal becomes a weak function of the size ratio in the (η_p, η_c) representation at higher colloid volume fractions, and, furthermore, binodals for different ξ cross one another

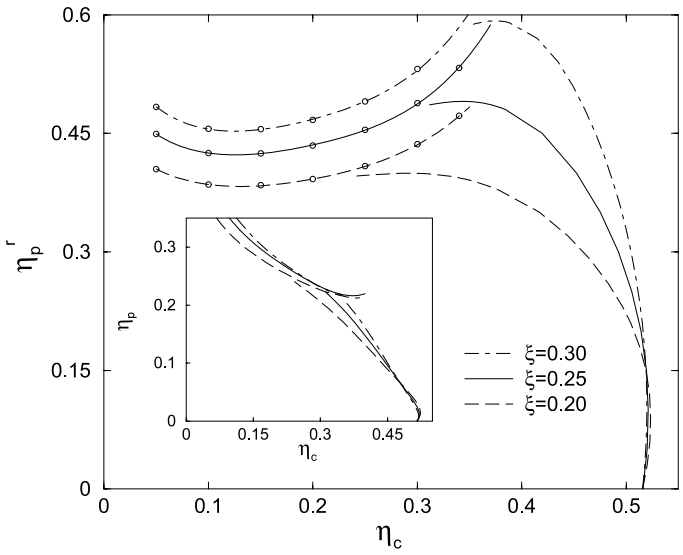

Figure 6. Glass transitions predicted by MCT using the PY colloid–colloid structure factor as input. Results are shown in terms of the polymer reference volume fraction η_p^r as a function of colloid volume fraction η_c for three different polymer–colloid size ratios, as labelled. The inset depicts the same data in terms of the polymer volume fraction η_p, based on the total sample volume.

in this region. Although difficult to see from the inset to figure 6, the PY spinodals exhibit the same trend. It should be noted, however, that while in qualitative agreement with experiments, the PY approximation cannot in general be trusted in delivering precise estimates of critical points [67]. However, judging from the phase diagram for $\xi = 0.34$ [51], which is reasonably close to the attraction ranges of interest here, the PY estimate for the value of η_p^r at the critical point is in close agreement but the critical colloid density is underestimated.

The glass transitions predicted by MCT are shown in figure 6. For $\eta_p^r = \eta_p = 0$ they start at the hard-sphere glass transition value, $\eta_c = 0.5159$ [10], given the PY structure factor input. For small values of η_p^r or η_p the transition tends to larger colloid volume fractions only to migrate toward lower η_c on increasing the polymer concentration further. It follows that there is a region of reentrant glass melting, studied in depth by experiment [19–21], computer simulation [19, 68, 69], and MCT [18, 19, 70, 71] for far shorter-range attractions where this behaviour is more pronounced and leads to isostructural glass–glass transitions.

Increasing the polymer concentration sufficiently leads to the MCT transitions meeting the PY spinodal on the liquid side. As seen, this occurs closer to the critical point when the attraction is of short range. Somewhat prior to encountering the spinodal the transitions become non-monotonic functions of η_p^r, suggesting that small-wavelength correlations are influencing the MCT predictions. This does not occur for shorter-range attractions, where the predictions are strictly governed by the large wavevector behaviour of $S_{cc}(k)$. Since it is unknown, on closing in on a critical point, at which point MCT should be replaced by a more complete theory, handling also the critical dynamics, predictions in this region are the least reliable.

A very detailed experimental phase diagram, identifying locations of not only equilibrium phase coexistence but also non-ergodic gel states, is available from the work of Ilett and co-workers [7] for $\xi \approx 0.24$. They based their study on nearly hard-sphere poly(methyl methacrylate) particles dispersed in a slightly-better-than-theta solvent for the added, non-

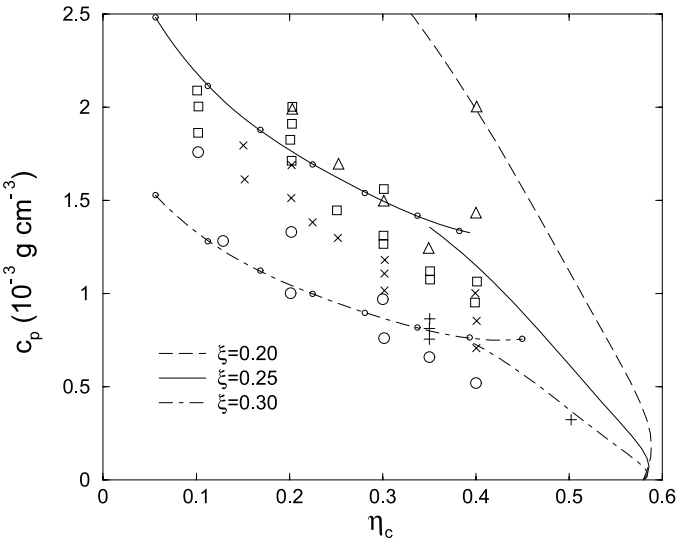

Figure 7. Comparison of MCT predictions for glass transitions against experiments on model colloid–polymer mixtures for $\xi \approx 0.24$, reproduced from [7], in terms of polymer mass concentration and colloid volume fraction. The symbols denote experimental data: (◯) fluid, (+) liquid + crystal, (□) gas + crystal, (×) gas + liquid + crystal, and (△) no visible crystallization. The lines are MCT predictions for different size ratios along with PY spinodals (marked by small circles as in figure 6), as labelled. Note that the colloid volume fraction in the theoretical predictions has been shifted to agree with the experimental glass transition value, ≈0.58 [14, 15, 17], namely $\eta_c = \eta_c^{\text{theory}} 0.58/0.516$.

adsorbing polystyrene polymer. The phase diagram is reproduced in figure 7, where colloidal fluid, gas–crystal, liquid–crystal, and three-phase coexistence regions have been determined as a function of added polymer mass concentration and colloid volume fraction. In addition, at the highest polymer concentrations crystallization was not detected. For the sake of showing the sensitivity of the MCT predictions to the size ratio, we have treated ξ as an adjustable parameter while keeping the polymer molecular weight M_w constant at the value quoted by Ilett *et al* [7]. The polymer mass concentration is then calculated as $c_p = 3M_w\eta_p/(4\pi(a\xi)^3 N_a)$, where a is the colloid radius and N_a is Avogadro's constant.

Figure 7 shows comparisons based on the MCT results for the glass transitions in figure 6 for $\xi = 0.20$, 0.25, and 0.30. They are shown along with the PY predictions for the spinodal. Although their locations do not vary too much in the (η_p, η_c) representation in figure 6, they separate from one another drastically because of the ξ^{-3} factor in the conversion from η_p to c_p. It is clear from the comparison that among the ξ values the best agreement is obtained by using $\xi = 0.25$ in the theory, which is nearly the same as that used in the experiments. For this size ratio the predicted glass transition line has a slope that agrees approximately with the cessation of crystal formation in the experiments.

Given the sensitivity of the prediction to the value of ξ and that it is a first-principles modelling effort, this is an encouraging result. However, this result also begs a number of questions. We have opted for treating the polymer in the simplest possible way. Polymer–polymer interactions and polymer deformability have not been included; rather, polymers are taken as phantom spheres. We have attempted to include effects of polymer–polymer interactions in the manner of Prasad [72], by which a non-ideal osmotic pressure and a concentration-dependent polymer size are inserted in the AO potential. This has the effect

of weakening the attraction relative to the standard AO potential. Consequently, predictions are shifted up in figures 6 and 7. In addition, MCT has a tendency to favour structural arrest over liquid states, whereby, for instance, the hard-sphere glass transition prediction in figure 7 is about 12% lower than the experimental value of ≈0.58 [14, 15, 17]. This effect is however mitigated to a large extent by using an accurate structure factor input [73, 74]. Considering a fuller range of MCT predictions for systems governed by the cage effect, quantitative discrepancies, with for example results from simulation [73, 75], remain, but predictions generally do not differ by more than ≈10–20%. However, for very short-range attractions, near the region of re-entry, quantitative agreement with computer simulations requires applying a substantial shift factor to the attraction strength [71]. It follows that 'correcting' the MCT glass transitions would likely require a shift of the predictions in the same direction as that brought on by modelling polymer–polymer interactions as in [72]. The agreement seen in figure 7 for $\xi = 0.25$ would markedly worsen if a substantial MCT correction were applied, particularly if combined with non-ideal polymer effects. On the other hand, if AO theory is a reasonable model for the case at hand, the results in figure 7 would certainly tolerate MCT corrections of the magnitude normally expected.

5. Conclusions

The AO model, perhaps the simplest, yet non-trivial, model of the depletion interaction, has been applied to colloid–polymer mixtures. The size ratio has been kept sufficiently small so that the two-component AO theory can be brought over to the effective one-component version, as verified by comparison of MC simulation of the two systems combined with particle insertions. PY theory for the one-component AO system yields near-quantitative predictions for colloid–colloid radial distribution functions and structure factors away from phase boundaries. Simple approximations have been suggested that produce reasonable predictions of the remaining radial distribution functions in the mixture. Mode-coupling theory based on the PY structural input produces predictions for glassy states in the phase diagram that are in good agreement with experiments on model colloid–polymer mixtures with $\xi \approx 0.24$.

Acknowledgments

Financial support from the Swedish Research Council is gratefully acknowledged. JB is a Royal Swedish Academy of Sciences Research Fellow, supported by a grant from the Knut and Alice Wallenberg Foundation.

Appendix

In this appendix we aim to derive some approximate results for the colloid–polymer and polymer–polymer pair correlation functions within the Asakura–Oosawa model. To this end we rely on the connection between the binary and the effective one-component descriptions, which becomes exact for small colloid–polymer size ratios, $\xi \leqslant 2\sqrt{3} - 1$. Furthermore, we exploit the fact that accurate results are obtained from Percus–Yevick integral equation theory for the one-component AO system [50].

We consider first Vrij's [38] formulation of the AO model, i.e., N_c hard-sphere colloids mixed with N_p interpenetrable polymers in a volume V at temperature T. Following Brader *et al* [40], but restricting the situation to homogeneous systems, we apply the semi-grand-canonical ensemble, in which the polymer fugacity z_p is fixed, along with N_c, V, and T. As

shown by them, the polymer degrees of freedom can be integrated out, leaving the following expression for the partition function:

$$\Psi = \frac{\mathrm{e}^{z_\mathrm{p} V(1-\eta_\mathrm{c}(1+\xi)^3)}}{N_\mathrm{c}!\Lambda_\mathrm{c}^{3N_\mathrm{c}}} \int \mathrm{d}\mathbf{R}^{N_\mathrm{c}} \mathrm{e}^{-\beta \sum_{i>j}^{N_\mathrm{c}} (\phi_\mathrm{cc}(R_{ij}) + \phi_\mathrm{AO}(R_{ij}))} \tag{6}$$

where $\xi \leqslant 2/\sqrt{3} - 1$ has been used to eliminate higher-order contributions. In equation (6), $\eta_\mathrm{c} = \pi\rho_\mathrm{c}\sigma_\mathrm{c}^3/6$ is the volume fraction of colloids, and Λ_ν is the thermal de Broglie wavelength of species ν. In the configuration integral the hard-sphere colloid–colloid potential, ϕ_cc, and the AO potential, ϕ_AO, appear as functions of the separation distance between colloids, R_{ij}. In the semi-grand-canonical ensemble the density distributions are defined as

$$\varrho_\mathrm{p}(\mathbf{r}_1) = \frac{\Psi^{-1}}{N_\mathrm{c}!\Lambda_\mathrm{c}^{3N_\mathrm{c}}} \sum_{N_\mathrm{p}=1}^{\infty} \frac{z_\mathrm{p}^{N_\mathrm{p}}}{(N_\mathrm{p}-1)!} \int \mathrm{d}\mathbf{r}_2 \cdots \mathrm{d}\mathbf{r}_{N_\mathrm{p}}\, \mathrm{d}\mathbf{R}^{N_\mathrm{c}} \mathrm{e}^{-\beta W} \tag{7}$$

$$\varrho^{(2)}(\mathbf{R}_1, \mathbf{r}_1) = \frac{\Psi^{-1}}{(N_\mathrm{c}-1)!\Lambda_\mathrm{c}^{3N_\mathrm{c}}} \sum_{N_\mathrm{p}=1}^{\infty} \frac{z_\mathrm{p}^{N_\mathrm{p}}}{(N_\mathrm{p}-1)!} \int \mathrm{d}\mathbf{r}_2 \cdots \mathrm{d}\mathbf{r}_{N_\mathrm{p}} \int \mathrm{d}\mathbf{R}_2 \cdots \mathrm{d}\mathbf{R}_{N_\mathrm{c}} \mathrm{e}^{-\beta W} \tag{8}$$

$$\varrho^{(2)}(\mathbf{r}_1, \mathbf{r}_2) = \frac{\Psi^{-1}}{N_\mathrm{c}!\Lambda_\mathrm{c}^{3N_\mathrm{c}}} \sum_{N_\mathrm{p}=2}^{\infty} \frac{z_\mathrm{p}^{N_\mathrm{p}}}{(N_\mathrm{p}-2)!} \int \mathrm{d}\mathbf{r}_3 \cdots \mathrm{d}\mathbf{r}_{N_\mathrm{p}}\, \mathrm{d}\mathbf{R}^{N_\mathrm{c}} \mathrm{e}^{-\beta W} \tag{9}$$

where $W = \sum_{i<j}^{N_\mathrm{c}} \phi_\mathrm{cc}(R_{ij}) + \sum_{i=1}^{N_\mathrm{c}} \sum_{j=1}^{N_\mathrm{p}} \phi_\mathrm{cp}(|\mathbf{R}_i - \mathbf{r}_j|)$ is the potential energy and lower-case coordinates have been used to distinguish polymer coordinates from upper-case colloid coordinates. Similar manipulations as led to equation (6) can be used to express the density distributions in terms of higher-order correlation functions; in particular, we find that

$$\frac{\rho_\mathrm{p}}{z_\mathrm{p}} = 1 + \rho_\mathrm{c} \int \mathrm{d}\mathbf{R}_1 f_{11} + \frac{\rho_\mathrm{c}^2}{2} \int \mathrm{d}\mathbf{R}_1\, \mathrm{d}\mathbf{R}_2 f_{11} f_{21} g_\mathrm{cc}(|\mathbf{R}_1 - \mathbf{R}_2|) \tag{10}$$

$$g_\mathrm{cp}(|\mathbf{R}_1 - \mathbf{r}_1|) = \frac{z_\mathrm{p}}{\rho_\mathrm{p}} \left((1 + f_{11}) \left[1 + \rho_\mathrm{c} \int \mathrm{d}\mathbf{R}_2 f_{21} g_\mathrm{cc}(|\mathbf{R}_1 - \mathbf{R}_2|) \right] + \frac{\rho_\mathrm{c}^2}{2} \int \mathrm{d}\mathbf{R}_2\, \mathrm{d}\mathbf{R}_3 f_{21} f_{31} g_\mathrm{ccc}^{(3)}(\mathbf{R}_1, \mathbf{R}_2, \mathbf{R}_3) \right) \tag{11}$$

$$g_\mathrm{pp}(|\mathbf{r}_1 - \mathbf{r}_2|) = \frac{z_\mathrm{p}}{\rho_\mathrm{p}} \left(1 + \rho_\mathrm{c} \int \mathrm{d}\mathbf{R}_1 f_{12} g_\mathrm{cp}(|\mathbf{R}_1 - \mathbf{r}_1|) + \frac{\rho_\mathrm{c}^2}{2} \int \mathrm{d}\mathbf{R}_1\, \mathrm{d}\mathbf{R}_2 f_{12} f_{22} g_\mathrm{ccp}^{(3)}(\mathbf{R}_1, \mathbf{R}_2, \mathbf{r}_1) \right) \tag{12}$$

where $f_{ij} = \mathrm{e}^{-\beta\phi_\mathrm{cp}(|\mathbf{R}_i - \mathbf{r}_j|)} - 1$ is the colloid–polymer Mayer function. Equation (10), or equivalently equation (5) since $\eta_\mathrm{p}^r = \pi z_\mathrm{p}\sigma_\mathrm{p}^3/6$, has been derived by Brader *et al* [40] and connects the binary and the effective one-component descriptions exactly as long as $\xi \leqslant 2/\sqrt{3} - 1$. As an intermediate result to equations (10)–(12), one readily obtains insertion formulae [76] for the quantities of interest:

$$\frac{\rho_\mathrm{p}}{z_\mathrm{p}} = \left\langle \mathrm{e}^{-\beta \sum_{i=1}^{N_\mathrm{c}} \phi_\mathrm{cp}(|\mathbf{R}_i - \mathbf{r}_1|)} \right\rangle_\mathrm{AO}$$

$$g_\mathrm{cp}(|\mathbf{r}|) = \frac{z_\mathrm{p}}{\rho_\mathrm{p}} \left\langle \mathrm{e}^{-\beta \sum_{i=1}^{N_\mathrm{c}} \phi_\mathrm{cp}(|\mathbf{R}_i - \mathbf{r}_1|)} V\delta(\mathbf{R}_1 - (\mathbf{r} + \mathbf{r}_1)) \right\rangle_\mathrm{AO}$$

$$g_\mathrm{pp}(|\mathbf{r}_1 - \mathbf{r}_2|) = \left(\frac{z_\mathrm{p}}{\rho_\mathrm{p}} \right)^2 \left\langle \mathrm{e}^{-\beta \sum_{i=1}^{N_\mathrm{c}} \phi_\mathrm{cp}(|\mathbf{R}_i - \mathbf{r}_1|)} \mathrm{e}^{-\beta \sum_{i=1}^{N_\mathrm{c}} \phi_\mathrm{cp}(|\mathbf{R}_i - \mathbf{r}_2|)} \right\rangle_\mathrm{AO}$$

where the averages are configurational averages in the one-component AO system. It follows that by inserting one or two polymer spheres in the colloid system one can determine the correlation functions by MC for any value of the fugacity. This has recently been made use of by Dijkstra *et al* [61], who also devised a Monte Carlo scheme for handling size ratios beyond $\xi \approx 0.1547$.

As an approximation, we neglect the higher-order terms in equations (11) and (12), in addition to neglecting terms deriving from non-pair-wise additivity of the AO potential, such that

$$g_{\mathrm{cp}}(|\mathbf{R}_1 - \mathbf{r}_1|) \approx \frac{z_\mathrm{p}}{\rho_\mathrm{p}} \mathrm{e}^{-\beta\phi_{\mathrm{cp}}(|\mathbf{R}_1-\mathbf{r}_1|)} \left(\frac{\rho_\mathrm{p}}{z_\mathrm{p}} + \eta_\mathrm{c}(1+\xi)^3 + \rho_\mathrm{c} \int \mathrm{d}\mathbf{R}_2 f_{21}(|\mathbf{R}_2 - \mathbf{r}_1|) g_{\mathrm{cc}}(|\mathbf{R}_2 - \mathbf{R}_1|) \right) \tag{13}$$

$$g_{\mathrm{pp}}(|\mathbf{r}_1 - \mathbf{r}_2|) \approx \frac{z_\mathrm{p}}{\rho_\mathrm{p}} \left(\frac{\rho_\mathrm{p}}{z_\mathrm{p}} + \eta_\mathrm{c}(1+\xi)^3 + \rho_\mathrm{c} \int \mathrm{d}\mathbf{R}_1 f_{12}(|\mathbf{R}_1 - \mathbf{r}_2|) g_{\mathrm{cp}}(|\mathbf{R}_1 - \mathbf{r}_1|) \right). \tag{14}$$

We have added and subtracted $\rho_\mathrm{p}/z_\mathrm{p}$ within the parentheses and used the leading-order result, $\rho_\mathrm{p}/z_\mathrm{p} = 1 - \eta_\mathrm{c}(1+\xi)^3$, which ensures that the correlation functions approach unity at large separations. However, by doing so we sacrifice the consistency in the opposite limit: $g_{\mathrm{pp}}(0) = z_\mathrm{p}/\rho_\mathrm{p}$. Reasonable results should accordingly be obtained when η_c and ξ are small. Once we have the colloid–colloid radial distribution function (cf below), a low-order approximation for the colloid–polymer and polymer–polymer radial distribution functions is obtained by completing the integrations in equations (13) and (14), which is readily done using bipolar coordinates.

A second approximation may be formulated, again by exploiting that accurate results are obtained for $g_{\mathrm{cc}}(R)$ in the effective one-component system using, for example, the Percus–Yevick closure. Here we begin with the Percus–Yevick closure of the Ornstein–Zernike equations for the binary AO mixture. Since the polymer–polymer direct correlation function vanishes in this case, we are left with the following Fourier-transformed equations:

$$h_{\mathrm{cc}}(k) = c_{\mathrm{cc}}(k) + \rho_\mathrm{c} c_{\mathrm{cc}}(k) h_{\mathrm{cc}}(k) + \rho_\mathrm{p} c_{\mathrm{cp}}(k) h_{\mathrm{cp}}(k) \tag{15}$$

$$h_{\mathrm{cp}}(k) = c_{\mathrm{cp}}(k)(1 + \rho_\mathrm{c} h_{\mathrm{cc}}(k)) \tag{16}$$

$$h_{\mathrm{pp}}(k) = \rho_\mathrm{c} c_{\mathrm{cp}}(k) h_{\mathrm{cp}}(k) \tag{17}$$

involving the Fourier-transformed total and direct correlation functions, $h_{\nu\mu}(k)$ and $c_{\nu\mu}(k)$. It is well known that these equations are rather poor at capturing correlations in the AO system, at least at high polymer concentrations [64]. The main problem arises from equation (15), which is readily seen in the limit $\rho_\mathrm{c} \to 0$, where it reduces to $h_{\mathrm{cc}}(R) = -\beta\phi_{\mathrm{AO}}(R)$ (with z_p replaced by ρ_p in the AO potential, consistent with the prescribed limit) in the range $\sigma_\mathrm{c} < R < \sigma_\mathrm{c}(1+\xi)$ rather than $\mathrm{e}^{-\beta\phi_{\mathrm{AO}}(R)} - 1$. The hyper-netted chain closure, on the other hand, does yield the correct dilute-limiting result. But rather than exploring alternatives to the Percus–Yevick closure, we replace equation (15) by the effective one-component equation, $h^{\mathrm{eff}}_{\mathrm{cc}}(k) = c^{\mathrm{eff}}_{\mathrm{cc}}(k) + \rho_\mathrm{c} c^{\mathrm{eff}}_{\mathrm{cc}}(k) h^{\mathrm{eff}}_{\mathrm{cc}}(k)$, where the colloids now interact also via the AO potential. This equation is solved subject to the one-component Percus–Yevick closure and the connection between the descriptions is made through equation (10), relating z_p to ρ_p. In the absence of approximating closures, and as emphasized by Dijkstra *et al* [64], $h_{\mathrm{cc}}(k) = h^{\mathrm{eff}}_{\mathrm{cc}}(k)$, so long as $\xi \leqslant 2/\sqrt{3} - 1$. It is easily verified also that the two descriptions are connected via Adelman's definition of the effective one-component direct correlation function [77], in this case given by

$$c^{\mathrm{eff}}_{\mathrm{cc}}(k) = c_{\mathrm{cc}}(k) + \rho_\mathrm{p} c_{\mathrm{cp}}(k)^2. \tag{18}$$

References

[1] Chen M and Russel W B 1991 *J. Colloid Interface Sci.* **141** 564
[2] Verduin H and Dhont J K G 1995 *J. Colloid Interface Sci.* **172** 425
[3] Rueb C J and Zukoski C F 1998 *J. Rheol.* **42** 1451
[4] Kapnistos M, Vlassopoulos D, Fytas G, Moretensen K, Fleischer G and Roovers J 2000 *Phys. Rev. Lett.* **85** 4072
[5] Gambaduro P, Venuti V, Mallamace F, Liao C, Tartaglia P and Chen S H 2001 *Colloids Surf.* A **183–185** 133
[6] Poon W C K, Selfe J S, Robertson M B, Ilett S M, Pirie A D and Pusey P N 1993 *J. Physique* II **3** 1075
[7] Ilett S M, Orrock A, Poon W C K and Pusey P N 1995 *Phys. Rev.* E **51** 1344
[8] Poon W C K 2002 *J. Phys.: Condens. Matter* **14** R859
[9] Stiakakis E, Petekidis G, Vlassopoulos D, Likos C N, Iatrou H, Hadjichristidis N and Roovers J 2005 *Europhys. Lett.* **72** 664
[10] Bengtzelius U, Götze W and Sjölander A 1984 *J. Phys. C: Solid State Phys.* **17** 5915
[11] Götze W 1991 *Liquids, Freezing and Glass Transition* ed J P Hansen, D Levesque and J Zinn-Justin (Amsterdam: North-Holland)
[12] Götze W and Sjögren L 1992 *Rep. Prog. Phys.* **55** 241
[13] Pusey P N and van Megen W 1986 *Nature* **320** 340
[14] Pusey P N and van Megen W 1987 *Phys. Rev. Lett.* **59** 2083
[15] van Megen W and Pusey P N 1991 *Phys. Rev.* A **43** 5429
[16] Götze W and Sjögren L 1991 *Phys. Rev.* A **43** 5442
[17] van Megen W and Underwood S M 1994 *Phys. Rev.* E **49** 4206
[18] Dawson K A, Foffi G, Fuchs M, Götze W, Sciortino F, Sperl M, Tartaglia P, Voigtmann T and Zaccarelli E 2000 *Phys. Rev.* E **63** 011401
[19] Pham K, Puertas A M, Bergenholtz J, Egelhaaf S U, Moussaïd A, Pusey P N, Schofield A B, Cates M E, Fuchs M and Poon W C K 2002 *Science* **296** 104
[20] Eckert T and Bartsch E 2002 *Phys. Rev. Lett.* **89** 125701
[21] Poon W C K, Pham K N, Egelhaaf S U and Pusey P N 2003 *J. Phys.: Condens. Matter* **15** S269
[22] Bergenholtz J and Fuchs M 1999 *Phys. Rev.* E **59** 5706
[23] Bergenholtz J, Poon W C K and Fuchs M 2003 *Langmuir* **19** 4493
[24] Sedgwick H, Egelhaaf S U and Poon W C K 2004 *J. Phys.: Condens. Matter* **16** S4913
[25] Foffi G, De Michele C, Sciortino F and Tartaglia P 2005 *Phys. Rev. Lett.* **94** 078301
[26] Lu P J, Conrad J C, Wyss H M, Schofield A B and Weitz D A 2006 *Phys. Rev. Lett.* **96** 028306
[27] Cates M E, Fuchs M, Kroy K, Poon W C K and Puertas A M 2004 *J. Phys.: Condens. Matter* **16** S4861
[28] Manley S, Wyss H M, Miyazaki K, Conrad J C, Trappe V, Kaufman L J, Reichman D R and Weitz D A 2005 *Phys. Rev. Lett.* **95** 238302
[29] Gast A P, Hall C K and Russel W B 1983 *J. Colloid Interface Sci.* **96** 251
[30] Gast A P, Hall C K and Russel W B 1983 *Faraday Discuss.* **76** 189
[31] Gast A P, Russel W B and Hall C K 1986 *J. Colloid Interface Sci.* **109** 161
[32] Lekkerkerker H N W, Poon W C K, Pusey P N, Stroobants A and Warren P B 1992 *Europhys. Lett.* **20** 559
[33] Chen Y L and Schweizer K S 2004 *J. Chem. Phys.* **120** 7212
[34] Bergenholtz J and Fuchs M 1999 *J. Phys.: Condens. Matter* **11** 10171
[35] Bergenholtz J, Fuchs M and Voigtmann T 2000 *J. Phys.: Condens. Matter* **12** 6575
[36] Asakura S and Oosawa F 1954 *J. Chem. Phys.* **22** 1255
[37] Asakura S and Oosawa F 1958 *J. Polym. Sci.* **33** 183
[38] Vrij A 1976 *Pure Appl. Chem.* **48** 471–83
[39] Roth R and Evans R 2001 *Europhys. Lett.* **53** 271
[40] Brader J M, Dijkstra M and Evans R 2001 *Phys. Rev.* E **63** 041405
[41] Frenkel D and Smit B 2002 *Understanding Molecular Simulation* (San Diego, CA: Academic)
[42] Manousiouthakis V I and Deem M W 1999 *J. Chem. Phys.* **110** 2753
[43] Miller M A, Amon L M and Reinhardt W P 2000 *Chem. Phys. Lett.* **331** 278
[44] Klein R and D'Aguanno B 1996 *Light Scattering, Principles and Development* ed W Brown (Oxford: Clarendon)
[45] Segre P N, Prasad V, Schofield A B and Weitz D A 2001 *Phys. Rev. Lett.* **86** 6042
[46] Prasad V, Trappe V, Dinsmore A D, Segre P N, Cipelletti L and Weitz D A 2003 *Faraday Discuss.* **123** 1
[47] Shah S A, Chen Y L, Schweizer K S and Zukoski C F 2003 *J. Chem. Phys.* **118** 3350
[48] Meijer E J and Frenkel D 1991 *Phys. Rev. Lett.* **67** 1110
[49] Meijer E J and Frenkel D 1994 *J. Chem. Phys.* **100** 6873
[50] Dijkstra M, Brader J M and Evans R 1999 *J. Phys.: Condens. Matter* **11** 10079
[51] Bolhuis P G, Louis A A and Hansen J P 2002 *Phys. Rev. Lett.* **89** 128302
[52] Warren P B, Ilett S M and Poon W C K 1995 *Phys. Rev.* E **52** 5205

[53] Aarts D G A L, Tuinier R and Lekkerkerker H N W 2002 *J. Phys.: Condens. Matter* **14** 7551
[54] Tuinier R, Aarts D G A L, Wensink H H and Lekkerkerker H N W 2003 *Phys. Chem. Chem. Phys.* **5** 3707
[55] Fuchs M and Schweizer K S 2002 *J. Phys.: Condens. Matter* **14** R239
[56] Schmidt M, Löwen H, Brader J M and Evans R 2002 *J. Phys.: Condens. Matter* **14** 9353
[57] Schmidt M, Denton A R and Brader J M 2003 *J. Chem. Phys.* **118** 1541
[58] Truskett T M, Torquato S, Sastry S, Debenedetti P D and Stillinger F H 1998 *Phys. Rev.* E **58** 3083
[59] Steinhardt P J, Nelson D R and Ronchetti M 1983 *Phys. Rev.* B **28** 784
[60] Auer S and Frenkel D 2004 *J. Chem. Phys.* **120** 3015
[61] Dijkstra M, van Roij R, Roth R and Fortini A 2006 *Phys. Rev.* E **73** 041404
[62] Hansen J P and McDonald I R 1986 *Theory of Simple Liquids* (London: Academic)
[63] Louis A A, Finken R and Hansen J P 1999 *Europhys. Lett.* **46** 741
[64] Dijkstra M, van Roij R and Evans R 2000 *J. Chem. Phys.* **113** 4799
[65] Lo Verso F, Pini D and Reatto L 2005 *J. Phys.: Condens. Matter* **17** 771
[66] Gallerani F, Lo Vecchio G and Reatto L 1985 *Phys. Rev.* A **31** 511
[67] Miller M A and Frenkel D 2004 *J. Chem. Phys.* **121** 535
[68] Puertas A M, Fuchs M and Cates M E 2002 *Phys. Rev. Lett.* **88** 098301
[69] Zaccarelli E, Foffi G, Dawson K A, Buldyrev S V, Sciortino F and Tartaglia P 2002 *Phys. Rev.* E **66** 041402
[70] Götze W and Sperl M 2003 *J. Phys.: Condens. Matter* **15** S869
[71] Sperl M 2004 *Phys. Rev.* E **69** 011401
[72] Prasad V 2002 Weakly interacting colloid polymer mixtures *PhD Thesis* Harvard University
[73] Foffi G, Götze W, Sciortino F, Tartaglia P and Voigtmann T 2004 *Phys. Rev.* E **69** 011505
[74] Voigtmann T, Puertas A M and Fuchs M 2004 *Phys. Rev.* E **70** 061506
[75] Nauroth M and Kob W 1997 *Phys. Rev.* E **55** 657
[76] Widom B 1963 *J. Chem. Phys.* **39** 2808
[77] Adelman S A 1976 *Chem. Phys. Lett.* **38** 567